Infrared Detection of a Phenylboronic Acid Terminated Alkane Thiol Monolayer on Gold Surfaces

Scott H. Brewer,† Angela M. Allen,† Simon E. Lappi,† Tyson L. Chasse,† Kimberly A. Briggman,‡ Christopher B. Gorman,† and Stefan Franzen*,†

Department of Chemistry, North Carolina State University, Raleigh, North Carolina 27695, and National Institute of Standards and Technology, Gaithersburg, Maryland 20899

Received June 12, 2003. In Final Form: October 5, 2003

Polarization modulation infrared reflectance absorption spectroscopy (PM-IRRAS) and infrared reflectance absorption spectroscopy (IRRAS) have been used to characterize the formation of a self-assembled monolayer of *N*-(3-dihydroxyborylphenyl)-11-mercaptoundecanamide) (abbreviated PBA) on a gold surface and the subsequent binding of various sugars to the PBA adlayer through the phenylboronic acid moiety to form a phenylboronate ester. Vibrationally resonant sum frequency generation (VR-SFG) spectroscopy confirmed the ordering of the substituted phenyl groups of the PBA adlayer on the gold surface. Solution FTIR spectra and density functional theory were used to confirm the identity of the observed vibrational modes on the gold surface of PBA with and without bound sugar. The detection of the binding of glucose on the gold surface was confirmed in part by the presence of a C−O stretching mode of glucose and the observed O−H stretching mode of glucose that is shifted in position relative to the O−H stretching mode of boronic acid. An IR marker mode was also observed at 1734 cm^{-1} upon the binding of glucose. Additionally, changes in the peak profile of the B−O stretching band were observed upon binding, confirming formation of a phenylboronate ester on the gold surface. The binding of mannose and lactose were also detected primarily through the IR marker mode at ∼1736 to 1742 cm^{-1} depending on the identity of the bound sugar.

Introduction

Surface-based assays have become highly prevalent in the development of high-throughput, sensitive biosensors.[1−3] This type of technology typically involves the attachment of a probe molecule to a surface that subsequently binds the target molecule from solution. For instance, the probe molecule can be a strand of ssDNA while the target is the complementary ssDNA.[4−6] A variety of surfaces such as glass,[2,7] gold,[3−5,8−12] and indium tin oxide[13−15] have been used to detect biologically relevant molecules such as DNA and peptides. These surface-based assays have utilized a number of techniques including electrochemistry,[13,16] fluorescence,[17−20] surface plasmon resonance (SPR),[3,8,10,21,22] and infrared spectroscopy.[6,11] However, fewer surface-based assays have been developed for the detection of carbohydrates or sugars. In solution, the well-known carbohydrate−phenylboronic acid interaction has been utilized for the detection of the presence of carbohydrates and sugars predominately by fluorescence.[23−28] However, fluorescence is not the preferred detection technique on a metallic surface because the metal surface quenches the fluorescence;[29] therefore, other techniques must be employed. Recently, a phenylboronic acid terminated alkane thiol monolayer on a gold surface was probed using SPR to detect the binding of various carbohydrates.[21,22] SPR is used to detect binding by measuring the optical effect of a change in the index of refraction on the surface adlayer. SPR does not provide

* To whom correspondence should be addressed. Phone: (919)-515-8915. Fax: (919)-515-8909.

† North Carolina State University.

‡ National Institute of Standards and Technology.

(1) Pease, A. C.; Solas, D.; Sullivan, E. J.; Cronin, M. T.; Holmes, C. P.; Fodor, S. P. A. *Proc. Natl. Acad. Sci. U.S.A.* **1994**, *91*, 5022−5026.
(2) Taton, T. A.; Mirkin, C. A.; Letsinger, R. L. *Science* **2000**, *289*, 1757−1760.
(3) Thiel, A. J.; Frutos, A. G.; Jordan, C. E.; Corn, R. M.; Smith, L. M. *Anal. Chem.* **1997**, *69*, 4948−4956.
(4) Herne, T. M.; Tarlov, M. J. *J. Am. Chem. Soc.* **1997**, *119*, 8916−8920.
(5) Steel, A. B.; Herne, T. M.; Tarlov, M. J. *Bioconjugate Chem.* **1999**, *10*, 419−423.
(6) Brewer, S. H.; Anthireya, S. J.; Lappi, S. E.; Drapcho, D. L.; Franzen, S. *Langmuir* **2002**, *18*, 4460−4464.
(7) Bai, X. P.; Li, Z. M.; Jockusch, S.; Turro, N. J.; Ju, J. Y. *Proc. Natl. Acad. Sci. U.S.A.* **2003**, *100*, 409−413.
(8) Nelson, B. P.; Grimsrud, T. E.; Liles, M. R.; Goodman, R. M.; Corn, R. M. *Anal. Chem.* **2001**, *73*, 1−7.
(9) Lee, H. J.; Goodrich, T. T.; Corn, R. M. *Anal. Chem.* **2001**, *73*, 5525−5531.
(10) Smith, E. A.; Erickson, M. G.; Ulijasz, A. T.; Weisblum, B.; Corn, R. M. *Langmuir* **2003**, *19*, 1486−1492.
(11) Frey, B. L.; Corn, R. M. *Anal. Chem.* **1996**, *68*, 3187−3193.
(12) Sauthier, M.; Carroll, R.; Gorman, C.; Franzen, S. *Langmuir* **2002**, *18*, 1825−1830.
(13) Armistead, P.; Thorp, H. *Anal. Chem.* **2000**, *72*, 3764−3770.
(14) Armistead, P.; Thorp, H. *Anal. Chem.* **2001**, *73*, 558−564.
(15) Popovich, N. D.; Yen, B. K.; Wong, S. S. *Langmuir* **2003**, *19*, 1324−1329.
(16) Steel, A. B.; Herne, T. M.; Tarlov, M. J. *Anal. Chem.* **1998**, *70*, 4670−4677.
(17) Fodor, S. P. A.; Read, J. L.; Pirrung, M. C.; Stryer, L.; Lu, A. T.; Solas, D. *Science* **1991**, *251*, 767−773.
(18) Lockhart, D. J.; Winzeler, E. A. *Nature* **2000**, *405*, 827−836.
(19) Bulyk, M. L.; Gentalen, E.; Lockhart, D. J.; Church, G. M. *Nat. Biotechnol.* **1999**, *17*, 573−577.
(20) Chee, M.; Yang, R.; Hubbell, E.; Berno, A.; Huang, X. C.; Stern, D.; Winkler, J.; Lockhart, D. J.; Morris, M. S.; Fodor, S. P. A. *Science* **1996**, *274*, 610−614.
(21) Lee, M.; Kim, T. I.; Kim, K. H.; Kim, J. H.; Choi, M. S.; Choi, H. J.; Koh, K. *Anal. Biochem.* **2002**, *310*, 163−170.
(22) Lee, M.; Hur, Y.; Kim, T.; Kim, K.; Kim, J.; Choi, H.; Koh, K. *Microchem. J.* **2002**, *72*, 315−321.
(23) Yoon, J.; Czarnik, A. W. *J. Am. Chem. Soc.* **1992**, *114*, 5874−5875.
(24) Wang, W.; Gao, S. H.; Wang, B. H. *Org. Lett.* **1999**, *1*, 1209−1212.
(25) Tong, A. J.; Yamauchi, A.; Hayashita, T.; Zhang, Z. Y.; Smith, B. D.; Teramae, N. *Anal. Chem.* **2001**, *73*, 1530−1536.
(26) Cao, H. S.; Diaz, D. I.; DiCesare, N.; Lakowicz, J. R.; Heagy, M. D. *Org. Lett.* **2002**, *4*, 1503−1505.
(27) Springsteen, G.; Wang, B. H. *Tetrahedron* **2002**, *58*, 5291−5300.
(28) DiCesare, N.; Pinto, M. R.; Schanze, K. S.; Lakowicz, J. R. *Langmuir* **2002**, *18*, 7785−7787.
(29) Demers, L. M.; Mirkin, C. A.; Mucic, R. C.; Reynolds, R. A.; Letsinger, R. L.; Elghanian, R.; Viswanadham, G. *Anal. Chem.* **2000**, *72*, 5535−5541.

10.1021/la035037m CCC: $27.50
Published on Web 05/15/2004

Scheme 1. Synthesis of *N*-(3-Dihydroxyborylphenyl)-11-mercaptoundecanamide), PBA

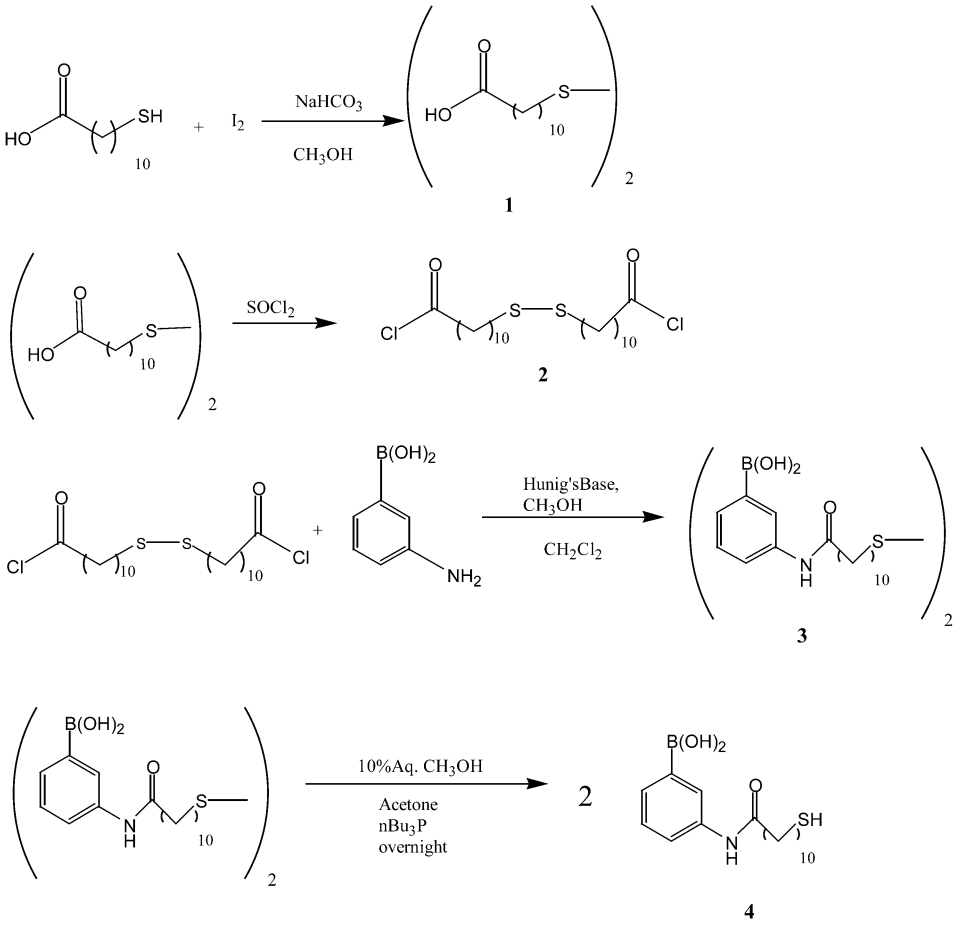

specific information on the orientation or surface order of bonding. Therefore, in these recent studies, reflectance infrared (IR) spectroscopy was used to confirm the presence of the dithiobis(4-butyrylamino-*m*-phenylboronic acid) monolayer on the surface.[21,22] However, no attempt was made to directly detect binding of a carbohydrate to the surface by reflectance IR spectroscopy.[21,22] We have recently demonstrated the detection of surface binding of DNA and proteins using reflectance IR both with and without polarization modulation.[6,30] Therefore, it is of interest to study the infrared spectroscopic signatures of surface-bound sugars as a prelude to studies of binding of lectins on surfaces.

In this study, polarization modulation infrared reflectance absorption spectroscopy (PM-IRRAS) and infrared reflectance absorption spectroscopy (IRRAS) were used for the fundamental characterization of a *N*-(3-dihydroxyborylphenyl)-11-mercaptoundecanamide) self-assembled monolayer (abbreviated PBA-SAM) on gold and for the characterization and detection of phenylboronate ester formation with various sugars. Infrared reflection spectroscopy is a rapid, nonintrusive method that can be used for the detection of sugars in biologically relevant concentrations. The PM-IRRAS technique does not require a fluorescent marker and provides information on the interaction between the phenylboronic acid moiety and the sugars. The binding of glucose, mannose, and lactose was detected and characterized in this study. The sugars studied here represent mono- and disaccharides consisting of six membered rings. The detection of sugar binding is through several modes including an IR marker mode at $\sim$1737 cm^{-1} for sugars bound to the phenylboronic acid moiety of PBA as well as changes in the frequency of B−O stretching modes that occur upon boronate ester formation. In principle, this information can be used to determine both bond strength and orientation of molecules on the surface. Vibrationally resonant sum frequency generation (VR-SFG) spectroscopy confirmed the formation of a well-ordered PBA-SAM on the gold surface.

Density functional theory was utilized to verify and assign the observed vibrational modes of PBA-SAMs on the gold surfaces. The present study demonstrates the feasibility of vibrational spectroscopic studies of sugar binding to surface groups that can have wide application in studies of cell and viral surfaces, binding by lectins and cell targeting agents.

Materials and Methods

Chemicals and Substrates. 3-Aminophenylboronic acid hemisulfate was purchased from Acros Organics.[36] Glucose, mannose, lactose (all sugars were D chirality), and other chemicals and reagents used in the synthesis of *N*-(3-dihydroxyborylphenyl)-11-mercaptoundecanamide) were purchased from Sigma-Aldrich.[36] Absolute ethyl alcohol (200 proof) (AAPER Alcohol)[36] was used for the preparation of the monolayer deposition and sugar solutions. Boric acid (^{11}B and ^{10}B isotopes) was received from Eagle Picher.[36] Evaporated gold substrates (with a Ti adhesion layer) were purchased from Evaporated Metal Films, Inc.[36]

Synthesis of *N*-(3-Dihydroxyborylphenyl)-11-mercaptoundecanamide). The synthesis of *N*-(3-dihydroxyborylphenyl)-11-mercaptoundecanamide) is shown in Scheme 1 and will be abbreviated PBA. 11-Mercaptoundecanoic acid (5 g, 22.9 mmol) was added to a suspension of methanol (5 mL), sodium bicarbonate (5.77 g, 68.7 mmol), and molecular iodine (2.91 g, 11.4 mmol) to yield disulfide **1** which precipitated from solution and was

(30) Unpublished results.

used without further purification. This molecule (4 g, 9.2 mmol) was converted to the bis-acid disulfide **2** by refluxing for 30 min in thionyl chloride (21.89 g, 184.0 mmol). The excess thionyl chloride was removed by distillation. Subsequently a substitution reaction was performed to give the bis-amide disulfide **3** where the brownish oil of **2** (4 g, 8.48 mmol) was added to a mixture containing 3-aminophenylboronic acid hemisulfate (3.16 g, 17 mmol) and *N*,*N*-diisopropylethylamine (7 mL). Reduction of **3** (1 g, 1.6 mmol) with tributylphosphine (1.58 mL) yielded the final product **4**. The identity and purity of the final product were confirmed by ^{1}H NMR, [(199.967 MHz, CD_3OD) δ 1.33 (s, 12H), 1.67 (m, 4H), 2.36 (t, 2H, $J = 7.3$ Hz), 2.66 (t, 2H, $J = 7.2$ Hz), 7.30 (m, 1H), 7.48 (m, 1H), 7.61 (m, 1H), 7.78 (m, 1H)], Fourier transform infrared spectroscopy (FTIR), and elemental analysis.

Monolayer Formation on Gold Surfaces. The gold substrates used to prepare the monolayers were first cleaned in a piranha solution (3:1 ratio of H_2SO_4 and H_2O_2) (*caution*: piranha solution reacts violently with organic chemicals), rinsed with 18 MΩ·cm deionized water (Barnstead E-Pure),[36] and dried with N_2 gas. The gold surfaces were then placed in a 100 mmol/L ethanolic solution of PBA overnight at room temperature. The surfaces were then rinsed with absolute ethanol and dried with N_2 gas. Some of the PBA-SAMs on gold were then exposed to a 3 mmol/L ethanolic solution of glucose, mannose, or lactose for 30 min at room temperature, rinsed with absolute ethanol, and dried with N_2 gas.

Polarization Modulation Infrared Reflection Absorption Spectroscopy (PM-IRRAS). The PM-IRRAS spectra were recorded on a Digilab FTS 6000 spectrometer[36] equipped with a step scan interferometer, a liquid nitrogen cooled narrow band MCT detector, a globar source, and a UDR-4 filter. The IR radiation was typically phase modulated at frequencies of 400 or 800 Hz at an amplitude of 1.0 λ HeNe or 2.0 λ HeNe while stepping at 0.5−2.5 Hz. A gold grid polarizer was used to obtain either s- or p-polarized radiaton, which was then modulated by a Hinds ZnSe photoelastic modulator (PEM) operating at 37 kHz and an amplitude of 0.5 λ (strain axis 45° to the polarizer) before reflecting off the sample at an incident angle of 80° from the surface normal. The spectra were recorded at room temperature at a resolution of 4 cm^{-1} and were the results of 1 scan with a spectral range of 900−4000 cm^{-1}. The digital signal processing (DSP) algorithm incorporated into the Digilab spectrometer software was used to obtain the spectra, which eliminates the need for a separate reference gold slide.

Infrared Reflection Absorption Spectroscopy (IRRAS). The reflectance FTIR spectra were recorded using a Spectra-Tech[36] grazing angle reflectance attachment in a Nicolet Magna-IR 860 FTIR[36] spectrometer. The angle of incidence used was 80° with respect to the surface normal. An infrared polarizer was used to obtain p (vertically)-polarized light. The spectra of the monolayers deposited on the gold surfaces were obtained by taking a ratio of the single beam spectra of the deposited material on a gold surface to one of a freshly UV/ozonized bare gold surface. The rotational lines from gaseous water were subtracted from these spectra. The FTIR spectrometer was equipped with a liquid nitrogen cooled MCT/A detector, and the spectra were recorded at a resolution of 2 cm^{-1} with a spectral range of 900−4000 cm^{-1}. All IR spectra were the result of 256 scans and were recorded at room temperature. High quality spectra in the 900−1800 cm^{-1} region of the monolayers on the gold surfaces were obtained by PM-IRRAS. However, due to the Bessel function nodes inherent in the PM-IRRAS spectra in the OH stretching region, IRRAS spectra were used in the 1800−4000 cm^{-1} region.

Single-Pass Attenuated Total Reflection Fourier Transform Infrared (ATR-FTIR) Spectroscopy. The solution single-pass ATR-FTIR spectra of phenylboronic acid, glucose, and glucose bound to PBA (3 mmol/L in ethanol) were taken using a PIKE Technologies[36] single-pass ATR attachment attached to a Digilab FTS 3000 FTIR spectrometer[36] equipped with a germanium crystal for single-pass attenuated total reflection (ATR). The spectrometer was equipped with a liquid nitrogen cooled MCT/A detector, and the spectra were recorded at a resolution of 4 cm^{-1} with a spectral range of 650−4000 cm^{-1}. The solutions were allowed to concentrate on the ATR element to increase the absorptive features of the molecule of interest. The absorption spectra were the result of 64 scans and were recorded at room temperature.

Vibrationally Resonant Sum Frequency Generation (VR—SFG) Spectroscopy. The experimental approach used in our broadband SFG measurements has been described in detail elsewhere.[31,32] Broadband (>250 cm^{-1} full width at half-maximum (fwhm)) IR pulses, derived from a ∼50 fs, 1 kHz, amplified Ti-sapphire laser system, were temporally and spatially overlapped with narrow-bandwidth (∼2 cm^{-1}) 810 nm (VIS) pulses at the sample. The reflected sum frequency light was collected, dispersed in a 0.33 m spectrograph, and detected with a scientific grade CCD array detector. This allowed the simultaneous acquisition of a >250 cm^{-1} wide SFG spectrum. In this work, the energy, beam diameter, and angle of incidence with respect to the surface normal of the coincident IR and VIS pulses were typically 3 μJ, 150 μm, 67° and 2 μJ, 250 μm, 45°, respectively. Pairs of half-wave plates and polarizers in the optical pathway were used to control the polarization of the IR, VIS, and SFG beams. All SFG spectra reported were taken with a ppp polarization combination, in which the IR, VIS, and detected SFG beams were polarized in the plane of incidence. The displayed spectra were normalized by the response of a freshly UV/ozonized bare Au film, which corrects for the intensity envelope of the broad-bandwidth IR pulse. All spectra are presented with the *x*-axis as the IR wavenumber, to allow easy comparison with linear vibrational spectroscopies.

Density Functional Theory (DFT) Calculations. The geometry optimization and vibrational frequency calculations of the various models were done using DFT as implemented in the quantum chemistry software program DMol3 (Accelrys, Inc.).[33,36] The calculations were performed at the North Carolina Supercomputer Center (NCSC) on the IBM RS/6000 SP.[36] These calculations were done in the gas phase using the DNP (double numerical plus polarization) basis set, the GGA (generalized gradient approximation) functional,[34] and the method of finite differences for calculating the vibrational frequencies. The Accelrys, Inc. software Insight II[36] was used to build the models and to visualize the eigenvector projections of the normal modes of vibration of the models.

Results and Discussion

IR Spectra and DFT Calculations of a Phenylboronic Acid Undecane Thiol SAM. The IR spectra of a PBA-SAM on a gold surface and PBA in solution are shown in Figure 1A−D, while the DFT calculated PBA IR spectrum is shown in panels E and F of Figure 1 for the low and high wavenumber regions, respectively. Figure 1 illustrates the formation of a PBA-SAM on a gold surface due to the presence of the characteristic vibrational modes of PBA that are verified in the solution IR spectrum of PBA. The identity of these observed vibrational modes was confirmed through the DFT calculations of the normal modes of vibration of PBA.

Figure 1A and Figure 1B show the PM-IRRAS and IRRAS of a PBA-SAM on a gold surface in the 950−1800 and 2750−3400 cm^{-1} regions, respectively. The PM-IRRAS and IRRAS spectra (Figure 1A,B) were recorded at an incident angle of 80°. These spectra show several key IR vibrational modes indicative of the presence of a PBA-SAM on the gold surface. A partial list of these vibrational modes along with mode assignments is given in Table 1.[37] A comparison of these surface FTIR spectra with the solution and DFT calculations was done to confirm the origin and assignment of the observed vibrational modes. The vibrational modes in Figure 1A include a mode at

(31) Richter, L. T.; Petralli-Mallow, T. P.; Stephenson, J. C. *Opt. Lett.* **1998**, *23*, 1594−1596.
(32) Yang, C. S. C.; Richter, L. J.; Stephenson, J. C.; Briggman, K. A. *Langmuir* **2002**, *18*, 7549−7556.
(33) Delley, B. *J. Chem. Phys.* **1990**, *92*, 508−517.
(34) Perdew, J. P.; Chevary, J. A.; Vosko, S. H.; Jackson, K. A.; Pederson, M. R.; Singh, D. J.; Fiolhais, C. *Phys. Rev. B* **1992**, *46*, 6671−6687.

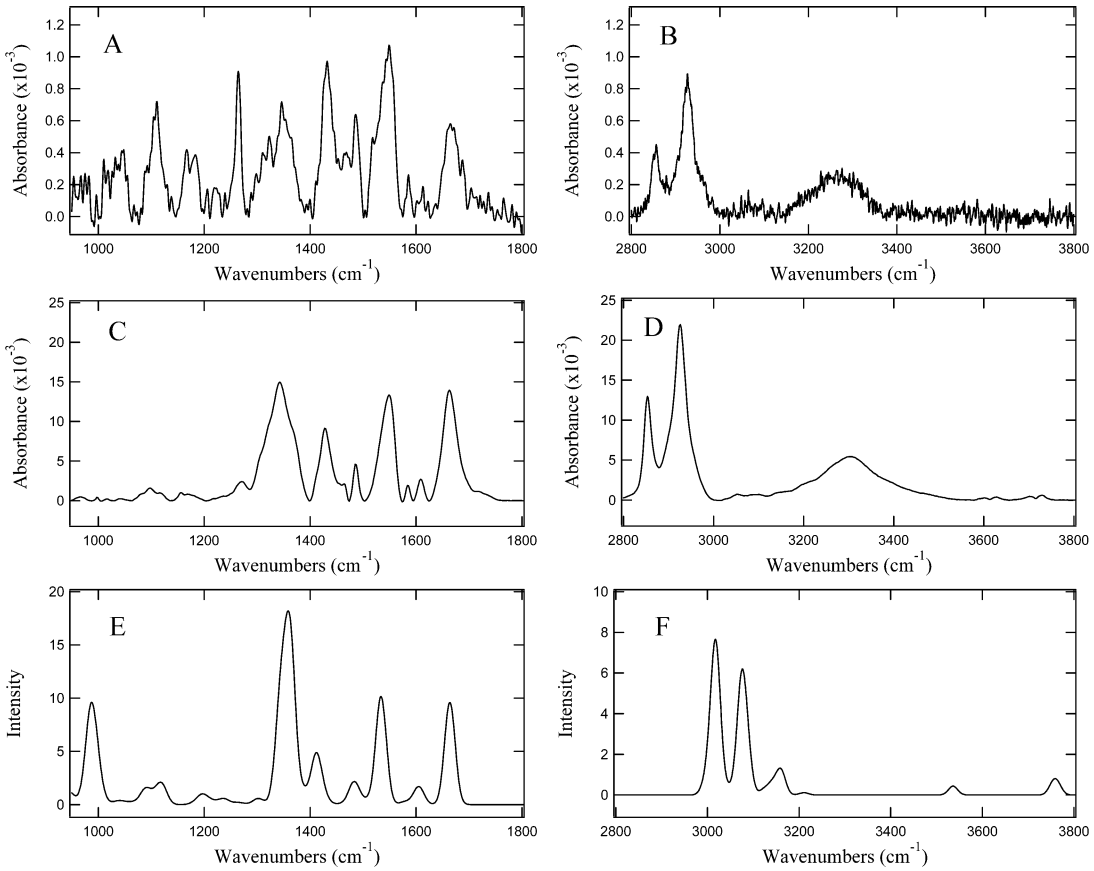

Figure 1. The PM-IRRAS (A) and IRRAS (B) spectra of a monolayer of PBA on a gold surface in the low and high wavenumber regions, respectively. The PM-IRRAS and IRRAS spectra were recorded at an incident angle of 80°. The IRRAS spectra were obtained with p-polarized IR radiation. Single-pass ATR-FTIR spectra of an initially 3 mmol/L PBA solution in ethanol allowed to concentrate on the ATR element are shown in the low (C) and high (D) wavenumber regions. DFT calculated low (E) and high (F) wavenumber regions of the infrared spectrum of PBA in the gas phase with a Gaussian width of 10 cm^{-1}.

Table 1. List of the Important Vibrational Modes and Mode Assignments Corresponding to PBA on a Gold Surface ((PM)-IRRAS), in Solution (Single-Pass ATR-FTIR), and Calculated by DFT

vibrational modes (cm^{-1})			
experimental			
(PM)-IRRAS	solution ATR-FTIR	calculated, DFT	mode assignment
1663	1663	1664	C═O stretch
1580	1549	1534	N−H bending
1430	1427	1412	C−C stretch (phenyl ring), B−O stretch
1342	1342	1362, 1344	B−O stretch
2856	2853	3017	symmetric CH_2 stretch
2927	2926	3076	asymmetric CH_2 stretch
3263	3304	3759	O−H stretch

1663 cm^{-1} that is predominately due to carbonyl stretching and some N−H bending, while the mode at 1580 cm^{-1} is primarily a N−H bending mode. The mode at 1430 cm^{-1} is likely due to a mixture of several motions including C−C and B−O stretching, while the band centered at 1342 cm^{-1} is likely due to vibrational modes involving B−O stretching motions. The mode at 1264 cm^{-1} is likely due to imperfections in the gold surface allowing the silicon oxide modes[35] of the glass substrate to be observed or that the skin depth of the gold is greater than the thickness of the gold film at these IR wavelengths. The mode at 1111 cm^{-1} is probably due to phenyl ring deformation modes. The predominant modes at 2856 and 2927 cm^{-1} are due to the symmetric and asymmetric stretching motions of the methylene groups in the alkane chain of PBA. The broad mode centered at 3263 ± 0.7 cm^{-1} (determined by Gaussian band fitting) is the result of O−H stretching motions of the $B(OH)_2$ moiety of PBA (with a possible component of N−H stretching). These modes and intensities are indicative of a PBA-SAM on the gold surface.

The single-pass attenuated total reflection Fourier transform infrared (ATR-FTIR) solution spectra of PBA (starting concentration of 3 mmol/L that was allowed to concentrate on the ATR element) are shown in Figure 1C and Figure 1D for the low and high wavenumber regions, respectively. These spectra verify that the observed vibrational modes in Figure 1A,B of a PBA-SAM on a gold surface are due to the PBA. The characteristic modes include the C═O stretch and N−H bending modes at 1663 and 1549 cm^{-1}, respectively. A mode at 1427 cm^{-1} is also present which is likely due to a combination of several vibrational motions in the molecule, while the B−O stretching modes are observed in solution by the band centered at 1342 cm^{-1}. There is a weak mode observed at 1098 cm^{-1} in the spectrum obtained in solution that appears to correspond to a much more intense mode observed in the surface spectrum. The methylene sym-

(35) Brewer, S. H.; Franzen, S. *J. Alloys Compd.* **2002**, *338*, 73−79.

(36) We identify certain commercial equipment, instruments, or materials in this article to adequately specify the experimental procedure. In no case does such identification imply recommendation or endorsement by the National Institute of Standards and Technology, nor does it imply that the materials or equipment identified are necessarily the best available for the purpose.

(37) The values of the experimental vibrational wavenumbers reported here were chosen to represent the highest intensity of the peak. The spectra were not fit except where noted.

metric and asymmetric stretching modes are present at 2853 and 2926 cm^{-1}. The BO−H stretching mode is centered at 3304 cm^{-1} (with a possible component of N−H stretching). These modes in Figure 1C,D clearly show that the modes observed experimentally on the surface (Figure 1A,B) are due to the presence of PBA on the surface.

The identities of the vibrational modes found in Figure 1A−1D were investigated by DFT calculations of PBA in the gas phase. These calculations involved the optimization of the structure of PBA and the calculation of the IR spectrum of this molecule. The eigenvalues (IR frequencies) and eigenvectors (motion of the atoms giving rise to an IR mode) allow the identification and confirmation of the atomic motions resulting in the observed IR modes of this molecule. The resulting DFT calculated IR spectra of PBA are displayed in Figure 1E and Figure 1F in the low (950−1800 cm^{-1}) and high (2800−3800 cm^{-1}) wavenumber regions with a 10 cm^{-1} Gaussian width, while the eigenvectors for several prominent modes are shown in the Supporting Information. The DFT calculated infrared spectrum closely resembles the spectrum obtained on the gold surface (Figure 1A and Figure 1B) and in solution (Figure 1C and Figure 1D), further verifying that these observed modes arise from vibrational modes of PBA. The DFT model shows that the mode at 1664 cm^{-1} is predominately a C═O stretching mode with some N−H bending character. These DFT model calculations do not predict any modes greater than 1664 cm^{-1}, which suggests that the low intensity intensity mode at 1717 cm^{-1} for PBA as observed in solution is not a normal mode of vibration but a combination mode. The mode at 1534 cm^{-1} is a N−H bending mode while the mode at 1412 cm^{-1} is the result of C−C stretching in the phenyl ring, B−O stretching, and several other smaller components. The DFT model calculates two intense modes at 1362 and 1344 cm^{-1} that are primarily due to B−O stretching motions.

The DFT model also calculates a mode at 1121 cm^{-1} due to phenyl ring deformation but with a low intensity. The model does show an intense phenyl-ring-breathing mode at 984 cm^{-1}, observed experimentally as a relatively weak band in the solution and surface FTIR spectra. The modes at 3017 and 3076 cm^{-1} are due to symmetric and antisymmetric CH_2 stretching motions of the methylene units of the alkane chain of PBA, respectively and two modes at 3158 and 3211 cm^{-1} are due C−H stretching of the phenyl ring. The DFT model also calculates modes at 3536 and 3759 cm^{-1} due to N−H and O−H stretching motions, respectively. As observed in Figure 1E and Figure 1F, the DFT calculated IR spectra overall agreed with experiment and aided in the assignment of the experimentally observed modes of PBA.

Isotopic Shift in B−O Stretching Vibrations Observed by IR Spectroscopy. To verify the identity of the boron−oxygen stretching motions in PBA, the two isotopes (^{11}B and ^{10}B) of boric acid were investigated. Figure 2A shows the single-pass ATR-FTIR spectra of solid boric acid ^{11}B (natural abundance) and ^{10}B, while Figure 2B shows the DFT calculated IR spectra of these two isotopes of boric acid ($B(OH)_3$) in the gas phase with a 30 cm^{-1} Gaussian width. The inset in Figure 2B shows the eigenvector projections for the two calculated normal modes of vibration for natural abundance boric acid in the 1250−1650 cm^{-1} region. These experimental and DFT calculated IR spectra of the two isotopes of boric acid illustrate the region where B−O stretching modes occur in agreement with the assignments for the B−O stretching modes for PBA above, accounting for the change in environment between PBA and boric acid. Figure 2A shows a broad transition in the 1250−1650 cm^{-1} region with

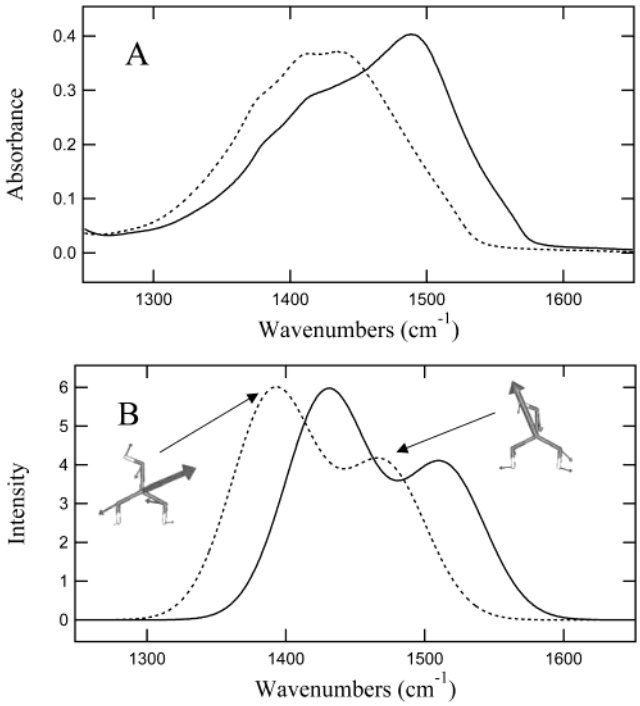

Figure 2. (A) Single-pass ATR-FTIR spectra of ^{11}B (dashed) and ^{10}B (solid) boric acid solids. (B) DFT calculated infrared spectra of ^{11}B (dashed) and ^{10}B (solid) boric acid in the gas phase with a Gaussian width of 30 cm^{-1}. (Inset: eigenvector projections of boric acid corresponding to the two modes of boric acid in the 1250−1650 cm^{-1} region.)

three prominent modes at approximately 1437, 1412, and 1376 cm^{-1} for ^{11}B. These two peaks shift to approximately 1488, 1417, and 1381 for ^{10}B. This shift is the expected shift to higher wavenumbers ($\tilde{\nu}$) for the ^{10}B boric acid spectra relative to ^{11}B due to the decrease in reduced mass of ^{10}B according to eq 1:

$$\tilde{\nu} = \frac{1}{(2\pi)c}\sqrt{\frac{k}{\mu}} \qquad (1)$$

where k is the force constant and μ is the reduced mass. Figure 2B shows that the DFT calculated IR spectra containing two intense modes in this region at 1471 and 1391 cm^{-1} for ^{11}B and at 1513 and 1430 cm^{-1} for ^{10}B boric acid. The agreement with the peak positions and peak shifts upon isotopic substitution are in agreement with the experimental FTIR spectra taking into account that the DFT IR spectra were calculated in the gas phase and therefore do not account for the packing in the solid material. The eigenvectors in the inset of Figure 2B illustrate the motions in the boric acid giving rise to these two modes which are predominately B−O stretching modes.

Spectroscopic Studies of Boronate Ester Formation. Figure 3A−J shows the surface, solution, and DFT calculated IR spectra of PBA with and without glucose bound. These spectra illustrate the detection of the formation of the boronate acid by the binding of glucose to the boronic acid moiety of a PBA-SAM on a gold surface through the observed characteristic vibrational modes of this molecule. These vibrational modes were verified by the solution IR spectroscopy, and the origins of the observed modes were confirmed through DFT calculations of the boronic acid and boronate ester species.

Figure 3A shows the PM-IRRAS spectra in the 950−1800 cm^{-1} region of a monolayer of PBA on a gold surface

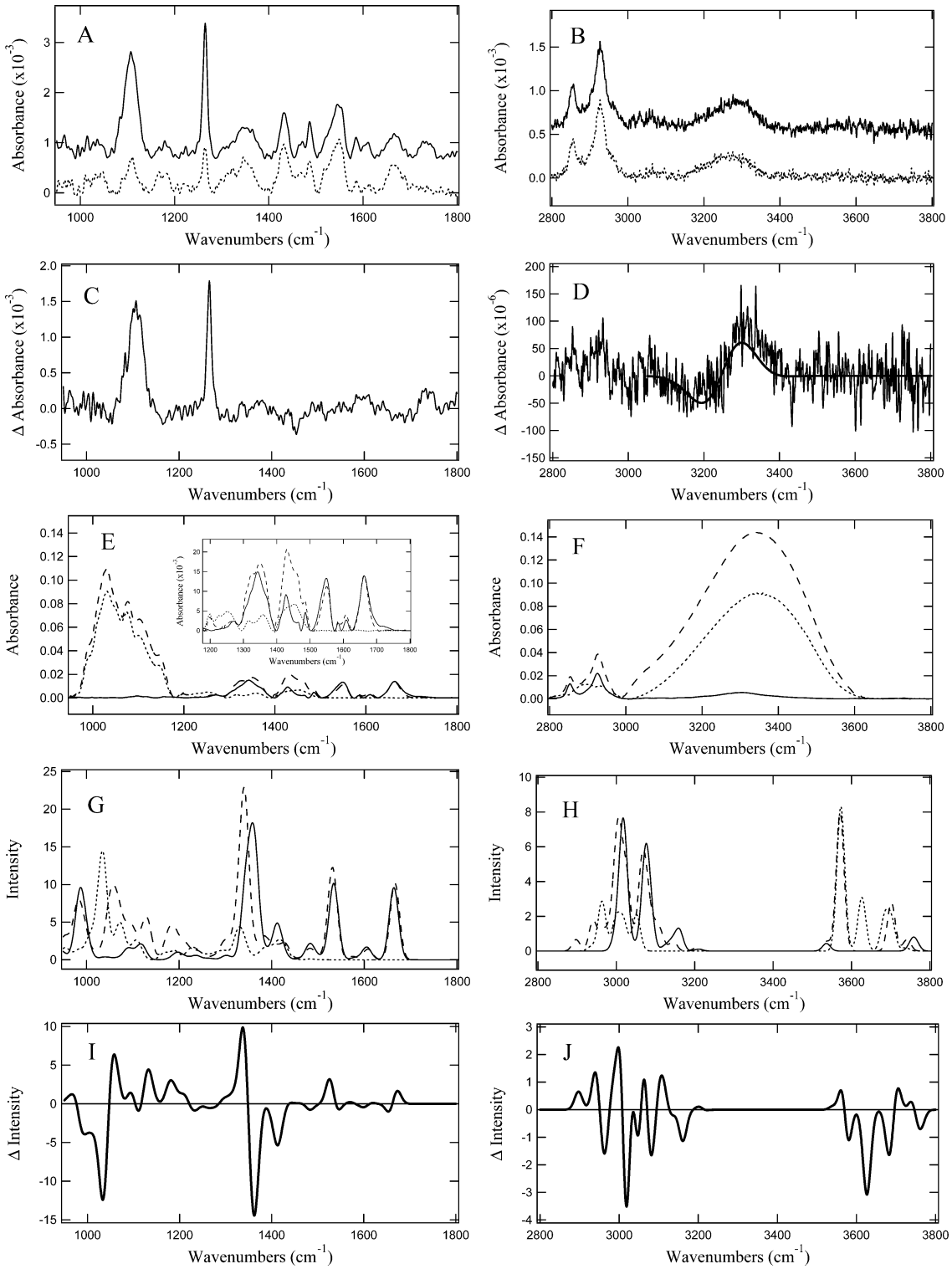

Figure 3. PM-IRRAS (A) and IRRAS (B) spectra of a monolayer of PBA exposed (solid spectrum) or unexposed (dashed spectrum) to a 3 mmol/L ethanolic solution of glucose for 30 min in the low (A) and high (B) wavenumber region on a gold slide recorded at an incident angle of 80°. The corresponding difference spectra for the low (C) and high (D) wavenumber regions are shown for glucose bound to a PBA-SAM on gold minus a PBA-SAM on gold. (The difference of the Gaussian fits in the O−H stretching region is shown in panel D.) Single-pass ATR-FTIR spectra solutions of PBA (solid), glucose (short dashed), and a 1:1 molar ratio of PBA and glucose (long dashed) are shown in the low (E) and high (F) wavenumber regions. DFT calculated infrared spectra of PBA (solid), glucose (short dashed), and glucose bound to PBA (long dashed) with a Gaussian width of 10 cm^{-1} in the low (G) and high (H) wavenumber regions. DFT calculated difference infrared spectra (I and J) calculated by the subtraction of the sum of the individual calculated IR spectra of glucose and PBA from the calculated IR spectra of glucose bound to PBA.

exposed (solid) or not exposed (dashed) to a 3 mmol/L solution of glucose in ethanol for 30 min, while Figure 3B shows the IRRAS spectra of the same two samples in the 2750−3400 cm^{-1} region. The corresponding difference spectra of bound minus unbound glucose to a PBA-SAM on gold are shown in Figure 3C and Figure 3D for the low and high wavenumber regions, respectively. The identification of the modes for the PBA-SAM on a gold surface is described above. The spectra corresponding to glucose bound to a PBA-SAM through the phenylboronic moiety

show the modes characteristic of PBA while several new vibrational modes and peak shifts occur upon sugar binding.

For instance, the C−O stretching mode from the six-member glucose ring is observed at 1107 cm^{-1} after the PBA monolayer was exposed to glucose, suggestive of the presence of glucose. Also, shifts and changes in peak profile occur in the B−O stretching modes around 1342 cm^{-1}, suggestive of glucose binding to the phenylboronic acid moiety of PBA. As before, the mode at 1264 cm^{-1} is likely due to silicon oxide stretching motions in the glass substrate[35] due to imperfections (scratches) in the gold surface or could be due to the skin depth of the gold layer being larger than the thickness of the gold film on the glass slide at these IR wavelengths. Hence the intensity differences observed for the 1264 cm^{-1} mode are primarily due to the number of imperfections (scratches or variation of gold film thickness) of the gold surface. Another significant difference in the PM-IRRAS spectrum upon glucose binding to a PBA-SAM on gold is the presence of a mode at 1734 cm^{-1}. This mode is likely a combination mode whose intensity is significantly increased upon binding of glucose relative to the other vibrational modes of this molecule compared to a PBA-SAM on a gold surface. Figure 3B shows the presence of the symmetric and asymmetric methylene stretching modes at 2857 and 2927 cm^{-1}, respectively, before and after glucose binding and a shift in the O−H stretching region. Upon glucose binding, the O−H stretching mode of boronic acid shifts ~11 cm^{-1} higher to a peak centered at 3274 ± 0.7 cm^{-1} (determined by Gaussian band fitting) indicative of the O−H stretching mode of glucose and the subsequent disappearance of the O−H stretching mode of the phenylboronic acid moiety of PBA prior to binding. The nature of the binding and conformation of the assignment of these modes is made below through DFT models and solution spectra of these species. Reflectance FTIR spectra therefore allow for the detection of glucose binding to a PBA-SAM on a gold surface and for structural information on the binding to be obtained.

To confirm that the vibrational modes of PBA and glucose-bound PBA on the gold surface are due to vibrations in these two molecules, solution ATR-FTIR spectra were recorded for both species. The single-pass ATR-FTIR spectra of a 3 mM ethanolic solution of PBA (solid), glucose (short dashed), and a 1:1 molar ratio of PBA and glucose (long dashed) in the low (A) and high (B) wavenumber region are shown in Figure 3E,F. The spectra were obtained by allowing these solutions to concentrate onto the ATR element before acquiring the spectra. The modes from PBA have already been assigned above. The most notable modes from glucose are the C−O stretching band centered at 1099 cm^{-1} with several modes with a C−O stretching component in the 950−1180 cm^{-1} region and the O−H stretching mode centered at 3352 cm^{-1}. The spectra of glucose bound to PBA show a shift in the O−H stretching mode from 3304 cm^{-1} of the boronic acid component of PBA to 3343 cm^{-1} of the O−H stretching mode of glucose bound to PBA. In addition, a large intensity increase in the O−H stretching mode with glucose bound relative to PBA without glucose bound was observed. However, this intensity difference is not observed on the gold surface likely due to the orientation of the O−H transition dipole moment relative to the surface. The B−O stretching modes are also shifted and have a different peak profile with glucose bound to PBA (phenylboronate ester) compared to PBA without glucose bound (phenylboronic acid). These two observations are suggestive of the formation of a phenylboronate ester. The C−O

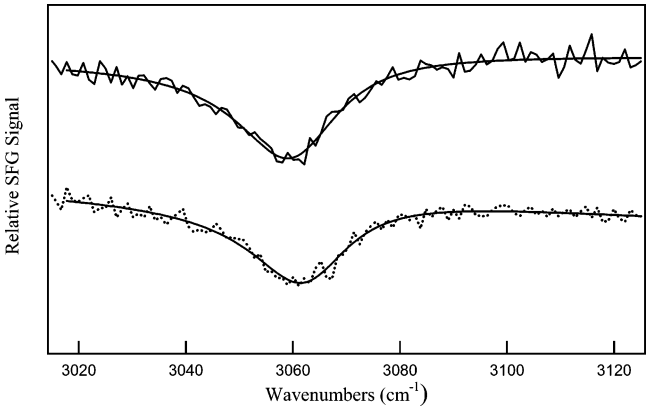

Figure 4. VR-SFG spectra of a PBA-SAM (dashed) on a gold surface exposed to a 3 mmol/L solution of glucose in ethanol for 30 min (solid) recorded with ppp polarization.

stretching mode of glucose is also evident in the glucose bound to PBA solution FTIR spectra. These differences between PBA and glucose bound to PBA are consistent with those observed on the gold surface (Figure 3A−D).

Figure 3G,H shows the DFT calculated infrared spectra of PBA (solid), glucose (short dashed), and glucose bound to PBA (long dashed) with a Gaussian width of 10 cm^{-1}. These calculations confirm the assignments of the observed vibrational modes of glucose bound to PBA of a gold surface and in solution. Figure 3I,J shows the difference infrared spectrum calculated by the subtraction of the sum of the individual calculated spectra of glucose and PBA from the calculated spectra of glucose bound to PBA. The origin of these calculated vibrational modes is illustrated by the eigenvector projections of selected normal modes of vibration of glucose bound to PBA shown in the Supporting Information. The model of glucose bound to PBA shows a 2 cm^{-1} shift to higher wavenumbers for the carbonyl stretching mode to 1666 cm^{-1}, whereas the N−H bending mode is shifted to lower wavenumbers by 3 cm^{-1} to 1531 cm^{-1} relative to free PBA. Figure 3G shows that the predominately B−O stretching modes in glucose bound to PBA are at 1341 and 1339 cm^{-1} compared to 1362 and 1344 cm^{-1} for free PBA. This shift is due to the binding of glucose through the $B(OH)_2$ moiety of the phenylboronic acid functional group of PBA. The C−O stretching mode of glucose in Figure 3G is calculated at 1131 cm^{-1} when glucose is bound to PBA. The calculated DFT frequencies also predict a glucose ring deformation mode at 1051 cm^{-1} when bound to PBA. Figure 3J shows that relatively small changes occur in the high wavenumber region of the calculated infrared spectrum of PBA with and without glucose bound compared to the low wavenumber region shown in Figure 3I. The IR spectroscopic differences calculated with these DFT models verify the experimental differences observed between PBA, glucose, and glucose bound to PBA and give insight into the origin of the observed normal modes of vibration. The DFT model of glucose bound to PBA does not predict a normal mode of vibration near 1734 cm^{-1}. A band at this wavenumber is clearly observed in the PM-IRRAS spectrum (intense) and to a lesser extent in the solution ATR-FTIR spectrum (low intensity). The lack of a calculated vibrational mode at 1734 cm^{-1} indicates that this band is a combination band (the sum of two normal modes of vibration). The DFT model shows several possible normal modes of vibration that could sum to give this combination mode. The position and peak profile of this combination mode change depending on the sugar bound (see below); therefore one of the normal modes giving rise to this

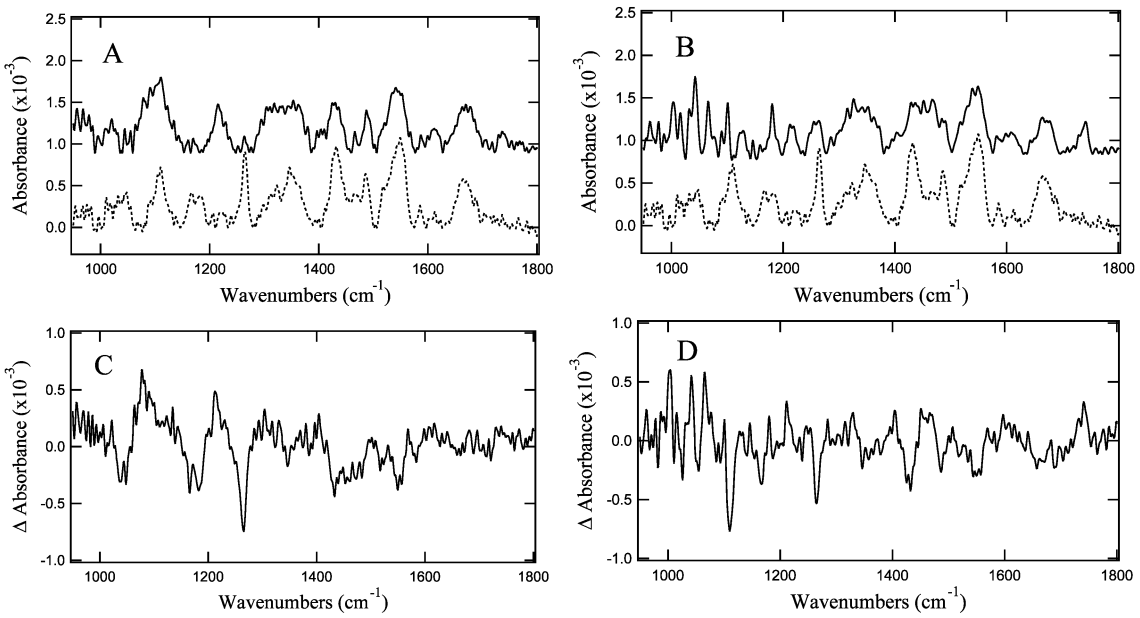

Figure 5. PM-IRRAS spectra of a monolayer of PBA exposed (solid) or not exposed (dashed) to a 3 mmol/L ethanolic solution of mannose (A) or lactose (B) for 30 min in the 950−1800 cm^{-1} region on a gold slide recorded at an incident angle of 80° and the corresponding difference sprectra for mannose (C) or lactose (D) bound to a PBA-SAM minus a PBA-SAM on gold.

combination mode probably involves the phenylboronic acid moiety of PBA. The DFT calculation does predict modes at 1341 cm^{-1} (B−O stretching) and 390 cm^{-1} (involves motions in PBA and glucose) that sum to give a calculated combination mode at 1731 cm^{-1}, which is in agreement with experimental data. These two fundamental modes are among the most intense calculated modes for glucose bound to PBA that is required for a combination band to be observed experimentally.

Figure 4 shows the VR-SFG spectra recorded with ppp polarization in the 3010−3125 cm^{-1} region of a PBA-SAM on a gold surface exposed (solid) or not exposed (dotted) to a 3 mmol/L solution of glucose in ethanol for 30 min. This region is shown so that the order of the substituted phenyl rings of the PBA-SAM could be investigated. The spectra are offset for clarity. These spectra demonstrate that the phenyl group of the PBA-SAM is ordered to the same extent both before and after exposure to a glucose solution by the presence of the aromatic C−H stretch mode presented in Figure 4. The peak positions in these spectra are identical within the 4 cm^{-1} resolution of the VR-SFG experiments. However, since this is a nonlinear spectroscopic technique, if the substituted phenyl groups were not well ordered in the PBA-SAM, little to no intensity in the VR-SFG spectra would be observed. The ordering of the PBA SAM was also investigated using DFT models on a PBA-SAM (see Supporting Information).

Figure 5A and Figure 5B show the PM-IRRAS spectra of a PBA-SAM exposed (solid) or not exposed (dashed) to mannose and the disaccharide lactose in the 950−1800 cm^{-1} region, respectively. The corresponding difference spectra of the sugar bound to the PBA-SAM minus the PBA-SAM is shown in Figure 5C and Figure 5D. These two spectra show that the detection of the binding of these two sugars can be made through the presence of the IR signature mode of sugar binding to a PBA-SAM on a gold surface centered at 1736 and 1742 cm^{-1} for mannose and lactose, respectively. The shift in the peak position of this mode further suggests that this combination mode is comprised of a normal mode of vibration sensitive to the phenylboronic acid moiety such as the B−O stretching motion. However, the intensity of this mode for mannose is much smaller than for glucose or lactose. Both of the sugars show a shift and a change in peak profile in the B−O stretching band around 1342 cm^{-1} of the PBA that results from binding of the sugar. The sugars are binding by formation of a phenylboronate ester as expected. There are also differences in the 1100 cm^{-1} region when a PBA-SAM was exposed to each sugar probably due to modes arising from the sugar bound to PBA.

Conclusions

A self-assembled monolayer of PBA was formed on a planar gold surface and was characterized and confirmed with PM-IRRAS, IRRAS, and VR-SFG spectroscopic techniques. The observed vibrational modes showed characteristics of PBA including the B−O stretching mode, amide modes (C═O stretching, N−H bending), C−N stretching modes, and O−H stretching modes. The identities of the observed modes of PBA on a gold surface were confirmed through solution single-pass ATR-FTIR spectra and density functional theory calculations. The subsequent binding of various sugars (glucose, mannose, and lactose) was detected and characterized by reflectance FTIR spectroscopy through several vibrational modes including the presence of an IR marker mode at between 1734 and 1742 cm^{-1} (depending on the identity of the sugar) upon phenylboronate ester formation of the PBA-SAM on a gold surface. A shift in the 1342 cm^{-1} boron−oxygen stretching mode was observed for phenylboronate ester formation for each sugar studied. The presence of the different sugars bound to the PBA-SAM on a gold surface was also seen in the C−O stretching mode around 1100 cm^{-1} which varied in intensity and peak profile depending on the sugar bound. For instance, both glucose and mannose exhibited a broad C−O stretching mode while lactose showed several more defined vibrational modes in this region.

Acknowledgment. Support and computational facilities were provided by the North Carolina Supercomputing Center. Scott Brewer was supported by NIH Biotechnology Training Grant T32-GM08776. The authors from North

Carolina State University would like to thank Digilabs for the use of the PM-IRRAS attachment.

Supporting Information Available: Single-pass ATR-FTIR spectra of glucose, mannose, and lactose; DFT optimized structure of a monolayer of PBA on gold; DFT eigenvector projections of PBA with and without glucose bound with the corresponding calculated normal mode wavenumbers. This material is available free of charge via the Internet at http://pubs.acs.org.

LA035037M